

Journal of Materials Chemistry A

Materials for energy and sustainability

Accepted Manuscript

This article can be cited before page numbers have been issued, to do this please use: X. Xu, S. Ma, S. Wang, J. Wu, Q. Li, N. lu, Y. liu, J. Yang, J. Feng and J. Zhu, *J. Mater. Chem. A*, 2020, DOI: 10.1039/D0TA01419B.



This is an Accepted Manuscript, which has been through the Royal Society of Chemistry peer review process and has been accepted for publication.

Accepted Manuscripts are published online shortly after acceptance, before technical editing, formatting and proof reading. Using this free service, authors can make their results available to the community, in citable form, before we publish the edited article. We will replace this Accepted Manuscript with the edited and formatted Advance Article as soon as it is available.

You can find more information about Accepted Manuscripts in the [Information for Authors](#).

Please note that technical editing may introduce minor changes to the text and/or graphics, which may alter content. The journal's standard [Terms & Conditions](#) and the [Ethical guidelines](#) still apply. In no event shall the Royal Society of Chemistry be held responsible for any errors or omissions in this Accepted Manuscript or any consequences arising from the use of any information it contains.

Dihydrazone-based Dynamic Covalent Epoxy Networks with High Creep Resistance, Command Degradability, and Intrinsic Antibacteria from Bioresources

Xiwei Xu,^{a,b} Songqi Ma,^{a*} Sheng Wang,^{a,c} Jiahui Wu,^b Qiong Li,^a Na Lu,^{a,c} Yanlin Liu,^a Jintao Yang,^b Jie Feng,^b Jin Zhu^a

^a Key laboratory of bio-based polymeric materials technology and application of Zhejiang province, Ningbo Institute of Materials Technology and Engineering, Chinese Academy of Sciences, Ningbo 315201, P. R. China

^b School of Materials Science and Engineering, Zhejiang University of Technology, Hangzhou 310014, P. R. China

^c University of Chinese Academy of Sciences, Beijing 100049, P. R. China

*Corresponding authors: (Songqi Ma) E-mail masongqi@nimte.ac.cn, Tel 86-0574-87619806

Abstract:

Covalent adaptable networks (CANs) provide a promising approach to the recycle issue of thermosets due to their dynamic cross-linked networks. However, CANs are susceptible to creep at relatively low temperatures, and their chemical stability is also inevitably doubted. Here, we designed novel dihydrazone CANs from cross-linking of a dihydrazone-containing epoxy monomer which was synthesized from the condensation of lignin derivative vanillin and hydrazinium hydrate, followed by reacting with epichlorohydrin. Beside the excellent malleability and reprocessability, the dihydrazone CANs exhibited high initial creep temperature of ~105 °C, which was ascribed to the superior stability of hydrazone bond at around 100 °C and favorable hydrazone exchangeability at elevated temperatures. Meanwhile, the degradation of the dihydrazone CANs exhibited temperature, solvent and acidity dependence. Moreover, on account of the high antibacterial property of hydrazone bond, the CANs presented high killing rate (95.8%) to Gram-negative bacteria (*E. coli*). Thus, this work disclosed an effective dynamic covalent motif for the development of CANs with excellent dimensional stability, chemical resistance and intrinsic antibacteria.

1. Introduction

Thermosets have been widely used as binders or matrices in coatings, adhesives, electronic packaging materials and composites, etc. and are also an extremely important part of the modern plastic and rubber industries.^{1, 2} Covalently cross-linked nature gives thermosets ideal properties including thermal stability, chemical resistance, creep resistance, but it also directly brings about exceedingly limited recycling options.³⁻⁸ The current main treatment of out-of-service thermosets is landfill which is the least preferred waste management approach according to the Environmental Protection Agency's (EPA) guidelines for solid waste management (1989). Other approaches such as grinding, solvolysis, combustion, and pyrolysis consume high energy and are de facto merely disposing instead of recycling the thermosets.⁸ To achieve a circular economy, it's urgent to develop method to efficiently recycle thermosets with low-energy consumption. Incorporating dynamic covalent bonds into thermosets to obtain covalent adaptable networks (CANs) is a promising route to address the recycle issue of thermosets. Especially after the pioneering work of vitrimers reported by Leibler and his coworkers,⁵ CANs have captured increasing attentions from academia and industry. So far, plenty of CANs have been designed based on dynamic chemistries or bonds such as transesterification,^{5, 9-11} DA/retro-DA reaction,^{12, 13} imine exchange,¹⁴⁻¹⁶ boronic ester or boroxine exchange,¹⁷⁻¹⁹ vinylogous urethanes/ureas,²⁰⁻²³ olefin metathesis,²⁴ carbamate,^{25, 26} carbonate,²⁷ hemiaminals,²⁸ 1,2,3-triazolium,^{29, 30} thiol-ene adducts,³¹ disulfides,³² siloxane,^{33, 34} silyl ether,^{35, 36} diketoenamine,⁴ diselenide,³⁷ thioacetal,³⁸ hindered urea bond,³⁹ acetal,^{40, 41} and so on.

Despite the rapid development, CANs are susceptible to creep as thermoplastics, which limits their utilization in applications including engineering plastics and structural materials requiring high dimensional stability. Even for the CANs with glass transition temperature (T_g) much higher than the topology freezing temperature (T_v) referring to the dynamic exchange reactions, creep could still occur at the temperature around T_v .¹⁶ Although few works have been done on enhancing the creep resistance of CANs, this aspect is attracting growing interests. One approach is incorporating permanent cross-links into CANs.⁴² Cash et al.⁴³ and Li et al.⁴⁴ designed CANs with different creep resistance and relaxation rates by adjusting the ratio of dynamic bonds to static bonds. Besides, Tang, Guo and coworkers⁴⁵ reported another method of improving the creep resistance of CANs through metal coordination which could also enhance the mechanical properties of CANs. Adjusting the types and contents of different catalysts should also be a method to increase the creep resistance. Leibler and coworkers,⁴⁶ Winne, Du Prez and coworkers²³ obtained a series of CANs with different relaxation rates and T_v s by adjusting the types and contents of different catalysts. Introducing physical cross-links could also enhance

the creep resistance of the CANs. Guan and coworkers³⁴ reported a silyl ether-based crystalline polyethylene vitrimer which exhibited good creep resistance below the melting point. Sumerlin and coworkers⁴⁷ prepared CANs using block copolymers which could produce microphase-separated network structure and enhance the creep resistance. Albeit the significant advances, it's still a challenge to achieve CANs combining high initial creep temperature above 100 °C and excellent malleability.

Dynamic covalent bonds could also impart the degradability to thermosets, but the chemical stability is inevitably doubted. It is a challenge to improve the stability of degradable thermosetting resins in daily use. In our previous work,⁴⁸ we designed degradable epoxy networks based on Schiff base conjugated with two benzene rings. On account of the stabilization from the conjugated benzene rings, the Schiff base epoxy networks exhibited superior temperature and acidity-controlled degradability, and excellent stability in common solvents, hydrothermal aging and thermal treatment. Nevertheless, the network rearrangement (or reprocess) could not be achieved.

Over the past few decades, antibiotic therapy has been regarded as a major advance in modern medicine because it plays a key role in reducing mortality in the treatment of severe infectious or chronic diseases.⁴⁹⁻⁵¹ However, with the abuse of antibiotics, the situation of the generation of antibiotic-resistant bacteria has become increasingly serious. Therefore, there is an urgent need for an antibiotic-free, highly effective antibacterial material to help us deal with daily bacterial infections. Recently, many schemes had been verified for antibacterial materials such as cationic polymers,^{52, 53} quaternary ammonium compounds,^{54, 55} hydrogels,^{56, 57} antibacterial peptides⁵⁸ and inorganic nanomaterials^{59, 60} which had achieved good results. However, there is no report on intrinsic antibacterial CANs.

Therefore, we synthesized a novel dihydrazone-containing epoxy monomer (HBE) and prepared dihydrazone CANs with high initial creep temperature, command degradability and excellent antibacteria. *To the best of our knowledge, this is the first report of dihydrazone CANs.* Besides, lignin derivative vanillin was used as the biorenewable raw material to prepare these dihydrazone CANs. The chemical structures of the synthesized compounds were characterized in detail. The thermal and mechanical properties, stress relaxation, reprocessing recyclability, creep resistance, degradability and the antibacterial properties were systematically investigated. The structure-property relationships were discussed as well. For comparison, the commonly used bisphenol A epoxy (DGEBA, trade name DER331) was studied as the control. All the chemical structures of epoxy monomers HBE and DER331, and hardeners isophorondiamine (IPDA) and poly(propylene glycol) bis(2-aminopropyl ether) (D400, average $M_n \approx 400$) were illustrated in **Fig. 1**.

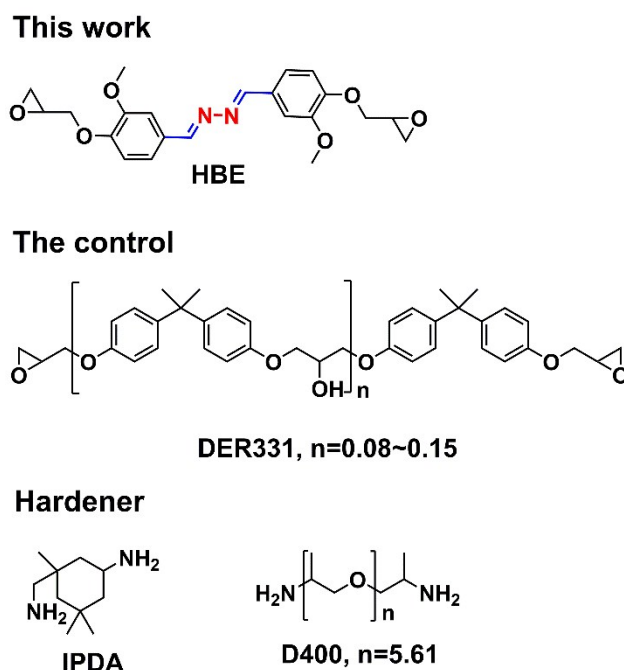


Fig. 1 Chemical structures of HBE, DER331, IPDA, and D400.

2. Experimental section

2.1 Materials

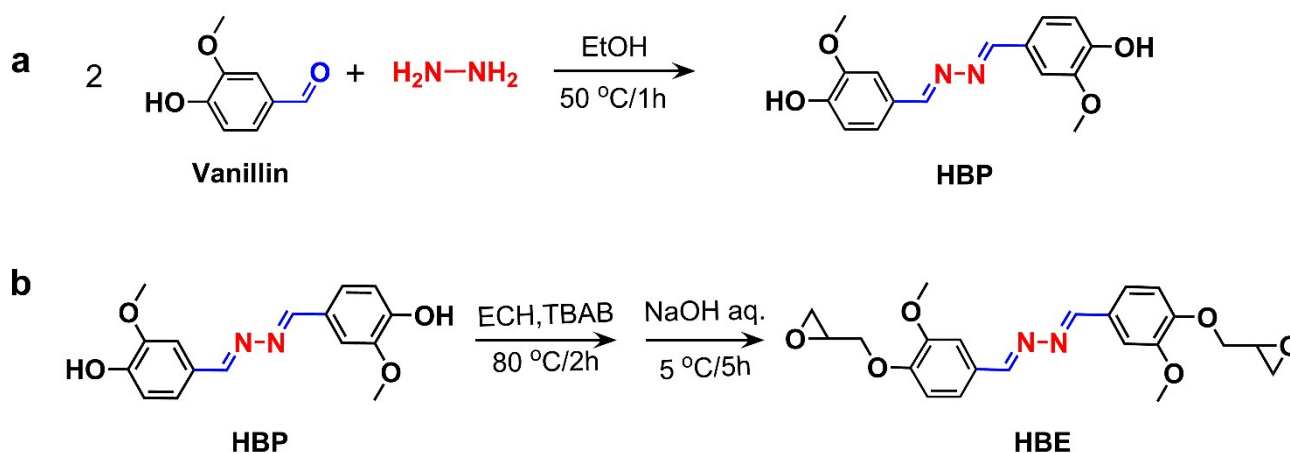
Isophorondiamine (IPDA), poly(propylene glycol) bis(2-aminopropyl ether) (D400, average $M_n \approx 400$), vanillin, hydrazinium hydrate solution (80%), phosphoric acid (>85 wt% in H_2O) and tetrabutylammonium bromide (TBAB) were purchased from Aladdin-reagent Co., China. Epoxy resin (DGEBA, trade name DER331, epoxide equivalent 182-192 $g\ eq^{-1}$) was supplied by DOW Chemical Company. Dimethyl sulfoxide (DMSO), N,N-dimethylformamide (DMF), petroleum ether (boiling range: 60-90 $^{\circ}C$), ethanol, methanol, acetone, tetrahydrofuran (THF), sodium hydroxide, acetic acid and epichlorohydrin (ECH) were obtained from Sinopharm Chemical Reagent Co., Ltd., China.

2.2 Synthesis of dihydrazone-containing epoxy monomer (HBE)

30.4 g (0.2 mol) of vanillin was dissolved in 100 mL of ethanol and poured into a 250-mL three-necked flask with a reflux condenser and a magnetic stirrer, and 6.25 g (0.1 mol) of hydrazinium hydrate solution (80%) was added dropwise to the above solution within half an hour at 50 $^{\circ}C$, then reacted at 50 $^{\circ}C$ for 1 h. After the reaction, the mixture was filtered to get a light yellow product (4,4'-(-hydrazine-1,2-diylidenebis(methanylylidene))bis(2-methoxyphenol) (HBP, 28.39 g) with a yield of approximately 94.6%.

Dihydrazone-containing epoxy monomer (HBE) was facily prepared by HBP through a two-step method. 6.02 g (0.02 mol) of HBP, 0.602 g (10 wt% of HBP) tetrabutylammonium bromide (TBAB) as the catalyst and 46.3 g (0.5 mol) of ECH were added to a 250 mL three-neck flask equipped with a reflux condenser and a magnetic stirrer, reacted at 80 °C for 1 h. Then the temperature of the reaction was kept below 5 °C by ice bath, and 5 g (0.05 mol) of 40 wt% sodium hydroxide (NaOH) aqueous solution was added dropwise to the system within 30 min. After that, 20 mL of chloroform was added, and the system was reacted for 5 h. When the reaction was completed, the mixture was washed by water for three times to obtain a yellow solution, and a white product HBE (6.99 g) with a yield of approximately 84.8% was obtained by precipitation of adding the solution dropwise to petroleum ether, and being dried at 80 °C for 12 h. The synthetic routes of HBP and HBE are illustrated in

Scheme 1.



Scheme 1 Synthetic routes of a) HBP and b) HBE.

¹H NMR (400 MHz, DMSO-*d*₆, ppm, HBP) δ = 9.71 (s, 1H), 8.58 (s, 1H), 7.46 (s, 1H), 7.32 - 7.20 (m, 1H), 6.88 (d, *J* = 8.1 Hz, 1H), 3.83 (s, 3H).

¹³C NMR (101 MHz, DMSO-*d*₆, ppm, HBP) δ = 165.23 - 158.80 (m, 2C), 150.33 (s, 1C), 148.43 (s, 1C), 127.48 - 124.77 (m, 1C), 124.98 - 122.12 (m, 2C), 117.55 - 114.69 (m, 2C), 113.04 - 107.68 (m, 2C), 58.35 - 53.20 (m, 2C).

¹H NMR (400 MHz, DMSO-*d*₆, ppm, HBE) δ = 8.65 (s, 1H), 7.51 (d, *J* = 1.8 Hz, 1H), 7.36 (dd, *J* = 8.4, 1.8 Hz, 1H), 7.09 (d, *J* = 8.4 Hz, 1H), 4.39 (dd, *J* = 11.4, 2.7 Hz, 1H), 3.97 - 3.77 (m, 4H), 3.41 - 3.34 (m, 1H), 2.92 - 2.82 (m, 1H), 2.72 (dd, *J* = 5.1, 2.6 Hz, 1H).

¹³C NMR (101 MHz, DMSO-*d*₆, ppm, HBE) δ = 163.37 - 158.80 (m, 1C), 153.65 - 150.15 (m, 1C), 150.15 - 146.65 (m, 1C), 130.77 - 124.77 (m, 1C), 125.63 - 119.83 (m, 1C), 114.47 - 111.97 (m, 1C), 111.61 - 108.11

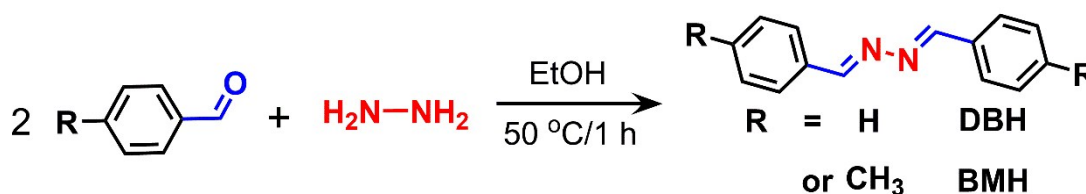
(m, 1C), 72.36 - 67.86 (m, 1C), 58.35 - 53.85 (m, 1C), 52.34 - 47.20 (m, 1C), 46.20 - 42.26 (m, 1C). View Article Online
DOI: 10.1039/D0TA01419B

HRMS (ES⁺) m/z calculated for HBE (C₂₂H₂₅N₂O₆ (M⁺ H⁺)) 413.16, found 413.17.

2.3 Synthesis of small-molecule model dihydrazones

Benzaldehyde (10.61 g, 0.1 mol) was dissolved in 100 mL of ethanol, and placed in a 250-mL flask with a reflux condenser and a magnetic stirrer, then 3.25 g (0.05 mol) of hydrazinium hydrate solution (80%) was added dropwise to the benzaldehyde solution, and reacted at 50 °C for 1 h. After the reaction, the mixture was cooled down and filtered to get a yellow product (1,2-di((E)-benzylidene)hydrazine) (DBH, 9.53 g) with a yield of 91.4%. 1,2-bis((E)-4-methylbenzylidene)hydrazine (BMH) with a yield of 93.2% was synthesized from p-methylbenzaldehyde and hydrazinium hydrate via the same method of DBH. The synthetic routes are shown in

Scheme 2.



Scheme 2 Synthetic routes of small-molecule model dihydrazones DBH and BMH.

¹H NMR (400 MHz, DMSO-*d*₆, ppm, DBH) δ = 8.70 (s, 1H), 7.86 (d, J=7.86, 2H), 7.48 (m, 2H).

¹³C NMR (101 MHz, DMSO-*d*₆, ppm, DBH) δ = 161.95 (s, 1C), 134.27 (s, 1C), 131.82 (s, 1C), 129.37 (s, 1C), 128.84 (s, 1C).

¹H NMR (400 MHz, DMSO-*d*₆, ppm, BMH) δ = 8.64 (s, 1H), 7.74 (d, J=7.9, 2H), 7.28 (d, J=7.9, 2H), 2.34 (s, 3H).

¹³C NMR (101 MHz, DMSO-*d*₆, ppm, BMH) δ = 161.68 (s, 1C), 141.78 (s, 1C), 131.67(s, 1C), 130.12-129.87(s, 1C), 128.88-128.64(s, 1C), 21.62(s, 1C).

2.4 Preparation of dihydrazone CANs

4.12 g (0.01 mol) of HBE and 2 g (0.005 mol) of D400 (or 0.85 g (0.005 mol) of IPDA) were dissolved in 10 mL of DMF, and held at 150 °C for 30 min. Then the solution was coated on a tinplate (cleaned by butanone) and reacted at 150 °C for 30 min until the solvent was evaporated completely to give pre-cured films, followed by post-curing at 100 °C for 2 h, at 150 °C for 2 h, and at 180 °C for 2 h in a vacuum oven. The cured thermosets

were named as HBE-D400 (or HBE-IPDA). DER331-D400 as the control was prepared by cross-linking DER331 with D400 through the same method. The well-cured films were removed from tinplate and used to measure the properties.

2.5 Reprocess of the dihydrazone CANs

The reprocess was carried out through a plate vulcanizer. The samples (HBE-D400 or HBE-IPDA) were cut into small pieces, and placed between two steel sheets covered with two polyimide films. Then, they were hot pressed at 180 °C under a pressure of 10 MPa for 40 min (HBE-D400) or 30 min (HBE-IPDA). After cooling to room temperature, the reprocessed samples were obtained.

2.6 Degradation of the dihydrazone CANs

Around 5 mg of sample (HBE-D400 or HBE-IPDA) was placed in approximately 10 mL solution of acid, organic solvent and deionized water in a 10-mL vial. The degradation behavior was investigated by adjusting the solvent ratio, acid, acid concentration, solvent and temperature. After being placed in a vacuum oven at 80 °C for 24 h, the samples were weighed and recorded as the initial weight. The sample was immersed in the corresponding solutions at 50 °C (or 23 °C). If the samples could be completely degraded within 48 h, the required time was recorded as the degradation time. If not, the remaining samples were washed with deionized water for three times, placed in a vacuum oven at 80 °C for 24 h for drying, weighed and recorded as the final weight. The degradation rate (v_d) was calculated by initial weight (w_i), final weight (w_f), and degradation time (t_d) via equation 1:

$$v_d = \frac{w_i - w_f}{t_d} \quad (1)$$

2.7 Static contact angle of the dihydrazone CANs

The static contact angle of the dihydrazone CANs was determined with a contact angle measuring system (OCA25, Dataphysics Instrument) using the sessile-drop method at room temperature (23 °C). Data were read at 1 min after deposition of 30 μ L distilled water or solvent.

2.8 Swelling measurement

The dihydrazone CANs were immersed in different solvents at 50 °C for 24 h. m_0 is the initial mass (dried) and m_1 is the mass after swelling; the swelling degree is calculated by $100\% \times (m_1 - m_0) / m_0$.

2.9 Antibacterial activity of the dihydrazone CANs

The antibacteria of the HBE-D400 and DER331-D400 was investigated by *Escherichia coli* (*E. coli*, Gram-negative). *E. coli* was cultured on Luria-Bertanni (LB, OXOID) agar plate for 14-16 h at 37 °C, then a single colony was picked

to the 40 mL LB at 37 °C. *E. coli* was incubated for approximately 12 h under shaking at 200 rpm and adjusted to an appropriate optical density of ~0.1 (*E. coli*) by dilution for reserving. The bacteria were killed on the surface of the samples by soaking the cleaned samples in 70% alcohol for 10 min, then removed the bacteria with phosphate-buffered solution (PBS). The treated samples were placed in the solution containing *E. coli* and then held at 37 °C for 24 h. Bacteria that were not adhered to the surface of the samples were washed away by drip washing three times with PBS. LIVE/DEAD BacLight kit (Thermo Fisher Scientific Inc., NY) was used to stain the samples for 10 min, and the stained samples were washed by PBS to remove the excessive dye. Finally, bacteria on the surface of samples were observed by Axio Observer A1 fluorescence microscope.

2.10 Characterization

¹H NMR and ¹³C NMR spectra were collected through an AVANCE III Bruker NMR spectrometer (Bruker, Switzerland) with DMSO-d₆ as the solvent. Time-of-flight mass spectrometry was performed by dissolving the sample in dichloromethane and measuring it on a TripleTOF 4600 time-of-flight mass spectrometer (AB Sciex, America) in positive ion mode. GC-MS spectra were carried out on a 7890B-5977A Gas Chromatography-mass Spectrometer (GC-MS) (Agilent, America) using dichloromethane as the solvent. Differential scanning calorimetry (DSC) was examined via a Mettler-Toledo Star 1 apparatus to investigate the glass transition temperatures (T_g s) of the CANs. The dihydrazone CANs (around 5 mg) were heated to 200 °C from 25 °C at a heating rate of 20 °C min⁻¹ and held at 200 °C for 5 min, then cooled to 0 °C from 200 °C at a cooling rate of 20 °C min⁻¹, and finally heated from 0 °C to 200 °C at a ramp rate of 20 °C min⁻¹. The second heating curves were used to obtain the T_g s of the CANs. Thermogravimetric analysis (TGA) of the CANs (approximately 5 mg for each sample) was performed on a Mettler-Toledo TGA/DSC1 thermogravimetric analyzer (Mettler Toledo, Switzerland) under a nitrogen atmosphere from 50 to 800 °C at a heating rate of 10 °C min⁻¹. The FT IR spectra were recorded using a Micro-FT IR Cary660 (Agilent, America) by absorbance mode. The dynamic mechanical analysis (DMA) was performed on a Q800 DMA (TA instruments, American) under the film tensile mode at a frequency of 1 Hz. Samples with dimensions of 25 mm (length) × 5 mm (width) × 0.3 mm (thickness) were used to test the dynamic mechanical properties from -50 °C to 200 °C at a ramp rate of 3 °C min⁻¹. Stress relaxation: samples with dimensions of 20 mm × 5 mm × 0.3 mm were preloaded by a 1 × 10⁻³ N force initially to keep straight. After reaching the testing temperature, it was allowed 10 min to reach thermal equilibrium. A constant strain (5%) was applied to each specimen throughout the test, and the relaxation modulus was recorded. Creep experiments: a constant stress of 1.0 MPa was applied to the specimen after temperature equilibration for 10 min followed by a 40 min recovery period. Tensile properties of the samples were performed on an Instron

5567 Electric Universal Testing Machine (Instron, America). The samples with dimensions of 60 mm (length) \times 5 mm (width) \times 0.3 mm (thickness) were measured with gauge length of 20 mm at a cross-head speed of 2 mm min⁻¹. For accuracy, the data were averaged from at least 5 specimens.

3. Results and discussion

3.1 Synthesis and chemical characterization of HBP, HBE, DBH, BMH and the dihydrazone CANs

HBP was synthesized by the condensation reaction of vanillin and hydrazinium hydrate according to the similar method in the literature,⁶¹ and then HBP was epoxidized by reacting with epichlorohydrin to achieve HBE. ¹H NMR, ¹³C NMR, FT IR and TOF-MS spectra were used to determine the chemical structures of HBP and HBE. As seen in **Fig. 2**, the chemical shift and integral area of the peaks in the ¹H NMR spectra, and the chemical shift and peak numbers in the ¹³C NMR spectra correspond exactly to the expected chemical structures of HBP and HBE. As shown in TOF-MS spectrum (**Fig. 3**), the molecular weight of HBE is consistent with the theoretical value. The melting points of HBP and HBE examined by DSC were 181 °C and 161 °C, respectively (**Fig. S1**, **Fig. S2**). These results are indicative of the successful synthesis of HBE. Small-molecule model dihydrazones DBH and BMH were synthesized by a similar method of HBP, and ¹H NMR and ¹³C NMR spectra were used to characterize these two compounds (**Fig. 4**). The chemical shift and integral area of the peaks in the ¹H NMR spectra and the chemical shift and peak numbers in the ¹³C NMR spectra are completely consistent with the chemical structures of DBH and BMH, which indicates that DBH and BMH were successfully synthesized.

The dihydrazone CANs were prepared from the curing reaction of HBE and hardeners (IPDA and D400). The completion of curing and retention of hydrazone group of the networks were characterized through FT IR spectra (**Fig. 5**). The characteristic absorption peak of hydrazone group at \sim 1620 cm⁻¹ was maintained, which is indicative of the successful introduction of hydrazone group into the CANs. The disappearance of the absorption peak for epoxy group at around 919 cm⁻¹ and the appearance of the absorption peak for hydroxyl group at around 3380 cm⁻¹ demonstrate the complete reaction of epoxy groups and amino groups.

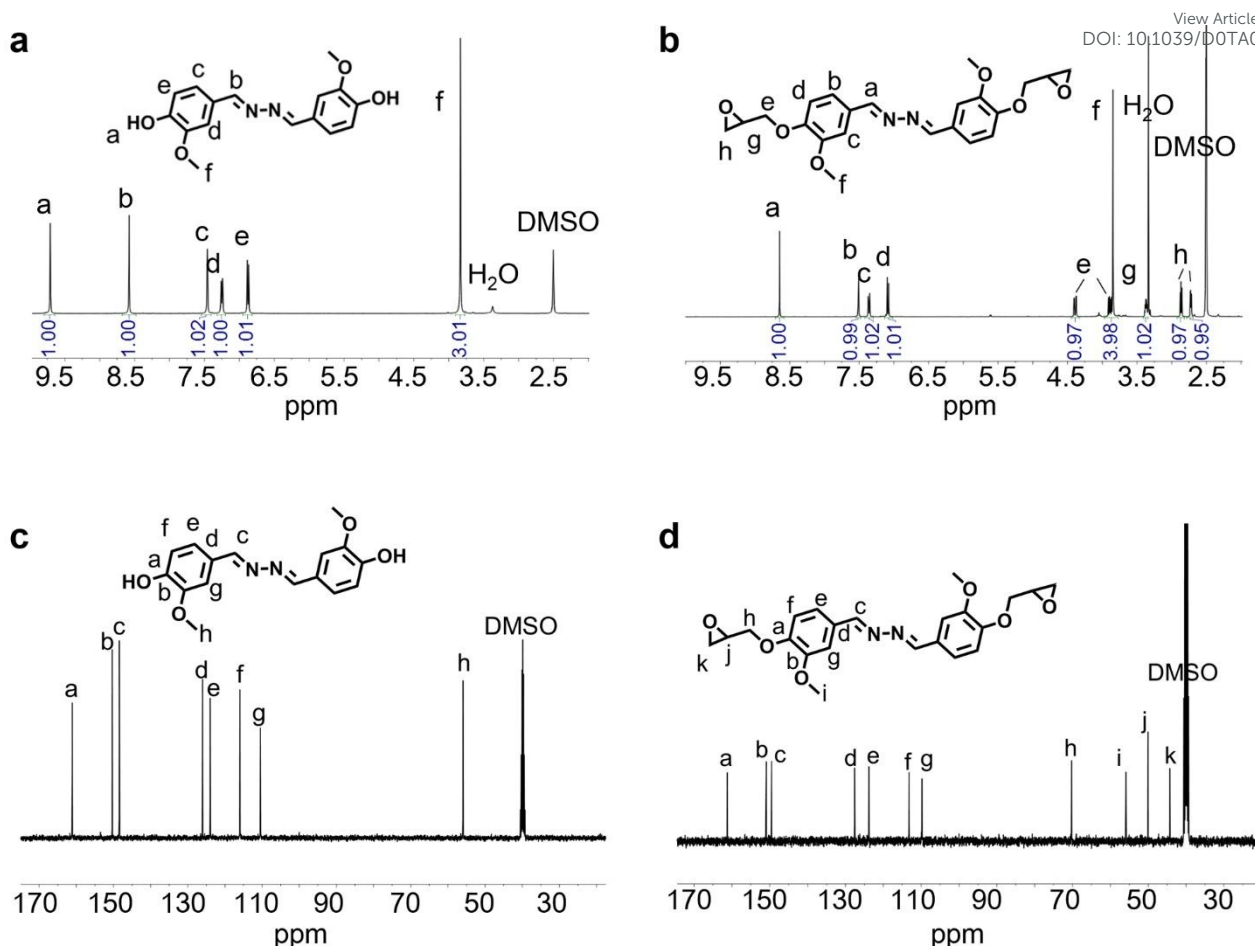


Fig. 2 ^1H NMR spectra of (a) HBP and (b) HBE; ^{13}C NMR spectra of (c) HBP and (d) HBE.

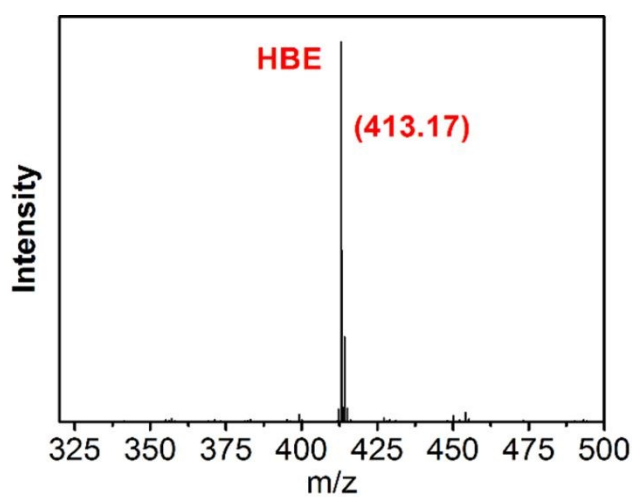


Fig. 3 TOF-MS spectrum of HBE.

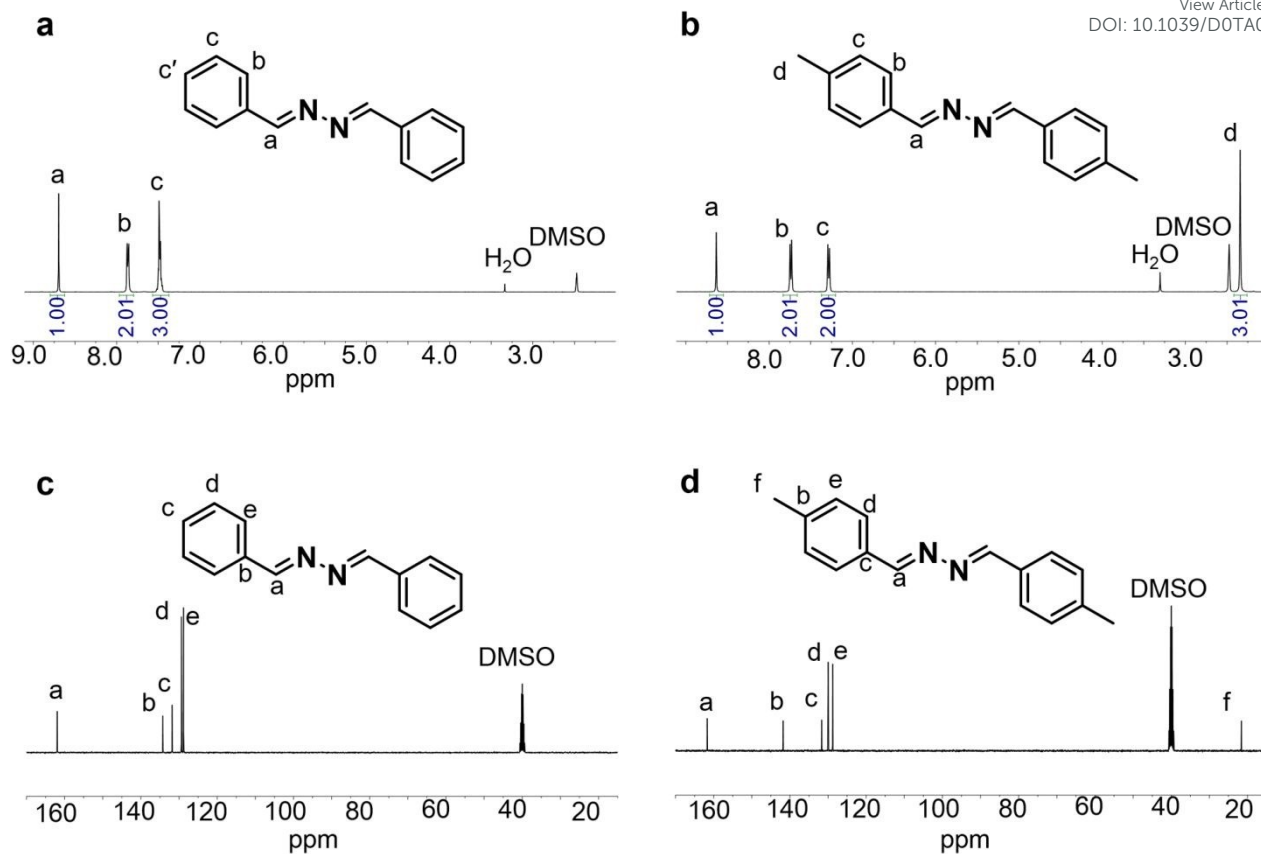


Fig. 4 ^1H NMR spectra of a) DBH and b) BMH; ^{13}C NMR spectra of c) DBH and d) BMH.

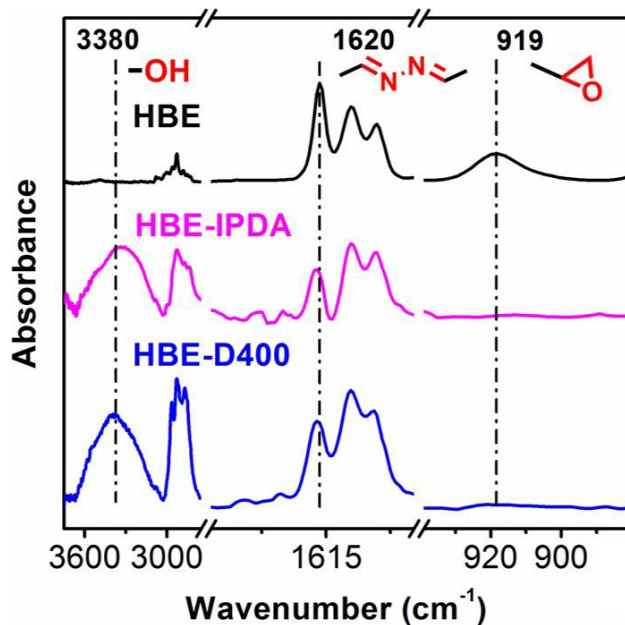


Fig. 5 FT IR spectra of HBE, HBE-D400 and HBE-IPDA.

3.2 Thermal and mechanical properties of the dihydrazone CANs

Glass transition temperature (T_g) is a significantly important performance index for thermosets, and to some

extent it determines the application of the thermosets. For comparison, HBE and commonly used bisphenol A epoxy (DER331) were cross-linked with the same curing agent (D400) to achieve HBE-D400 and DER331-D400, respectively. To facilitate discussion of the phenomenon of the creep in different situations, HBE was also cross-linked with a relatively rigid hardener IPDA to obtain T_g above topology freezing temperature (T_v).

In this paper, DSC and DMA were used to characterize the T_g s of the dihydrazone CANs (**Fig. 6** and **Table 1**). Obviously, cross-linked with the same curing agent, HBE-D400 exhibited higher T_g than DER331-D400. This is mainly attributed to the rigid conjugated structure of the hydrazone group in HBE-D400. HBE-IPDA has the highest T_g among these thermosets because of its highest cross-link density (calculate from equation 2 and 3, M_c , the average molecular weight between cross-link points, reflected the theoretical cross-link density, n and M respectively represent the molarity and molar mass of the components in the epoxy formulations; and ν_e reflected the actual cross-link density, E' is the plateau modulus in the rubbery state at $T_g + 30$ °C, R is the gas constant, and T is the Kelvin temperature of $T_g + 30$ °C) and the higher rigidity of IPDA segment than D400 segment.⁶²⁻⁶⁴ Owing to the excellent stability brought by its conjugated structure, hydrazone group is different from ordinary Schiff base, and the dihydrazone CANs (HBE-IPDA and HBE-D400) did not exhibit a significant increase in storage modulus at around 200 °C as Schiff base CAN,¹⁶ which would expand the potential applications of these dihydrazone CANs.

$$M_c = \frac{n_{\text{epoxy}} \cdot M_{\text{epoxy}} + n_{\text{hardener}} \cdot M_{\text{hardener}}}{n_{\text{hardener}}} \quad (2)$$

$$E' = 3\nu_e RT \quad (3)$$

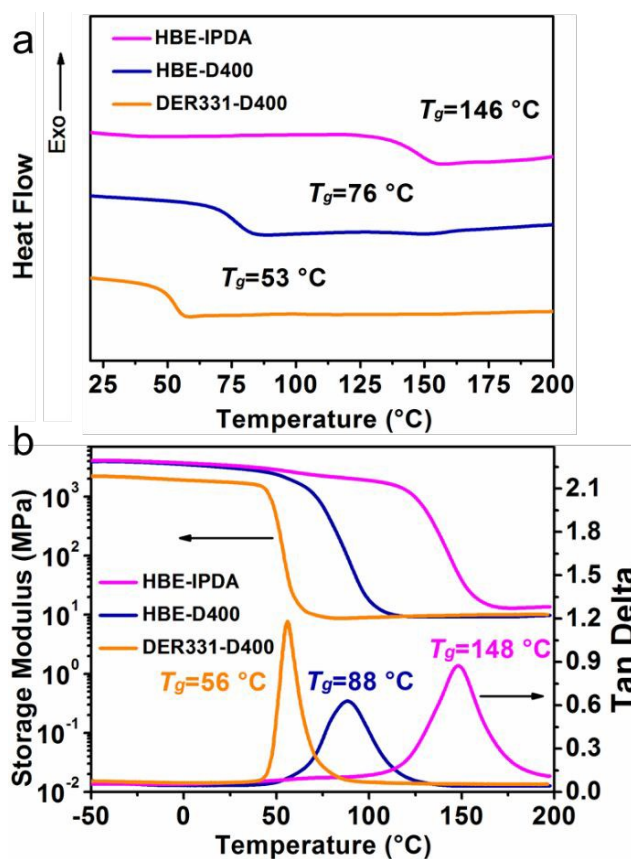


Fig. 6 a) DSC and b) DMA curves of HBE-IPDA, HBE-D400 and DER331-D400.

Table 1 Glass transition temperature (T_g), average molecular weight between cross-link points (M_c), storage modulus at $T_g + 30$ °C (E') and cross-link density (ν_e) of HBE-IPDA, HBE-D400 and DER331-D400.

Sample	T_g (°C)		M_c (g mol ⁻¹)	E' (MPa)	ν_e (mol m ⁻³)
	DSC	DMA			
HBE-IPDA	146	148	995	13.02	1239
HBE-D400	76	88	1225	9.47	1051
DER331-D400	53	56	1146	8.77	1068

Fig. 7 and **Table 2** present the mechanical properties of the cross-linked epoxy resins. With the same curing agent, the cross-link density of DER331-D400 was slightly higher than that of HBE-D400, however, Young's modulus and tensile strength of HBE-D400 were obviously higher than those of DER331-D400. This is attributed to the higher rigidity of the conjugated dihydrazone-containing structure and its related hydrogen bonding.¹⁶ Using IPDA as hardener, HBE-IPDA presented excellent mechanical properties with Young's

modulus of 1912 MPa and tensile strength of 97 MPa because of the high cross-link density, which is suggestive of the potential of HBE as a monomer for preparing high-performance thermosets.

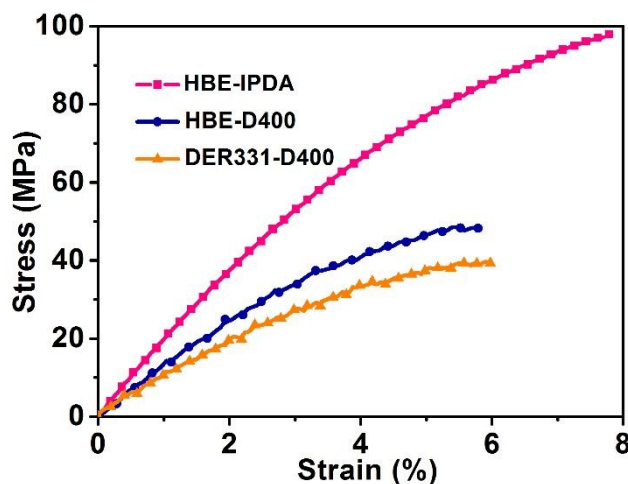


Fig. 7 Representative tensile stress-strain curves of HBE-IPDA, HBE-D400 and DER331-D400.

Table 2 Tensile properties of HBE-IPDA, HBE-D400 and DER331-D400.

Sample	Young's modulus (MPa)	Tensile strength (MPa)	Elongation at break (%)
HBE-IPDA	1912±51	97±2	7.9±0.3
HBE-D400	1637±46	53±4	5.9±0.2
DER331-D400	1186±14	36±3	6.1±0.3

3.3 Malleability and creep resistance of the dihydrazone CANs

Stress relaxation is a crucial feature of CANs, which makes them reprocessable. Here, stress relaxation tests of HBE-D400 and HBE-IPDA were carried out at elevated temperatures (170-185 °C) by monitoring the decrease of stress over time at constant strain (5%) (**Fig. 8a** and **Fig. 8b**). The characteristic relaxation time (τ^*) refers to the time required for the relaxation modulus to decrease to $1/e$ of the initial modulus. Although HBE-D400 owns lower cross-link density, it exhibited longer τ^* than HBE-IPDA. It is mainly due to its high molecular weight of hardener, resulting in the reduced content of hydrazone group and the increased molecular weight between cross-link points, which therefore reduced the rate of network rearrangement. It was clear that τ^* decreased with the increase of the test temperature, and the hydrazone exchange followed the characteristic CANs' Arrhenius behavior as defined by equation 4 (**Fig. 8c**).⁴⁶

$$\tau^*(T) = \tau_0 \exp(E_a/RT) \quad (4)$$

where τ_0 is the Arrhenius prefactor, R is the gas constant, and T is the experimental temperature. The E_a s (activation energy of the bond exchange process) of HBE-D400 and HBE-IPDA were calculated to be 95 kJ mol⁻¹ and 93 kJ mol⁻¹, respectively. The E' of HBE-D400 from 170 °C to 185 °C is 9.47 MPa, and that of HBE-IPDA in the same temperature range is 13.02 MPa (Fig. 6). T_v was defined as the temperature when η is 10¹² Pa, τ^* s at T_v of HBE-D400 and HBE-IPDA are calculated to be 3.9 × 10⁵ s and 2.7 × 10⁵ s, respectively. Using these values and equation (3) and (4), T_v was computed to be 109 °C for HBE-D400 and 105 °C for HBE-IPDA, detailed calculations are summarized in the supporting information.

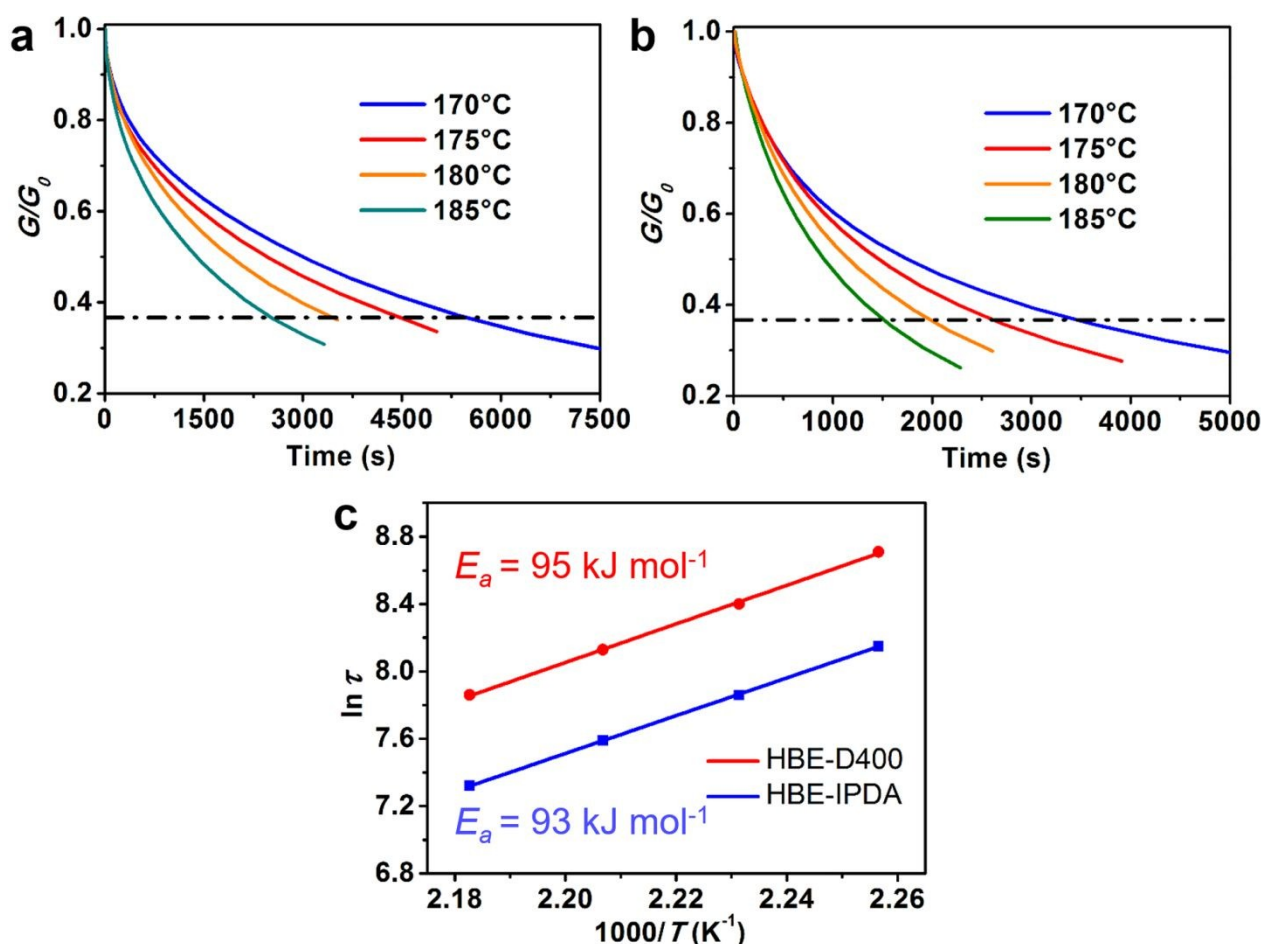


Fig. 8 Stress relaxation curves of a) HBE-D400 and b) HBE-IPDA at different temperatures. c) The fitted curves between $\ln(\tau^*)$ and $1000/T$, and the calculated E_a s of HBE-D400 and HBE-IPDA.

Creep resistance is a crucial indicator for polymers to be as engineering plastics or structure materials. As an engineering plastics, T_g should be above 100 °C⁶⁵ to guarantee the dimensional stability before 100 °C. As

shown in **Fig. 9** and **Fig. S3**, there was no creep phenomenon for DER331-D400 at 150 °C, it indicates that thermosets without reversibly covalent bonds will not creep. On account of the dynamic covalent bonds, CANs are susceptible to creep at relatively low temperature. For CANs, the maximum service temperature seems to be decided by the topology freezing temperature (T_v). Even for the CAN with T_g much higher than its T_v , the creep could occur at the temperature around T_v .¹⁶ Thus, creep analysis at different temperatures was subjected to these CANs for further exploration of the creep resistance. For the dihydrazone CANs HBE-D400 and HBE-IPDA, their T_v s are 109 °C and 105 °C, respectively, corresponding to the 100% strain recovery during the creep tests (no creep) at 105 °C for HBE-D400 (**Fig. 9a**) and at 100 °C for HBE-IPDA (**Fig. 9b**). This suggests that both HBE-D400 and HBE-IPDA possessed high initial creep temperature (or maximum service temperature) above 100 °C, which is higher than that (around 70 °C) of the conventional Schiff base CAN.¹⁶ This result is also better than the reported vitrimers with relatively high creep resistance, including the silyl ether-based vitrimer which has good creep resistance at 80 °C³⁴ and the boronic ester-based vitrimers modified by metal-ligand coordination.⁴⁵ For sake of disclosing the nature of the high creep resistance, small-molecule model dihydrazones DBH and BMH were used to investigate the hydrazone exchange reaction. DBH and BMH could react to produce a new dihydrazone BMBH following a metathesis mechanism (**Fig. 10a**). 0.208 g (0.001 mol) of DBH and 0.236 g (0.001 mol) of BMH were dissolved in 10 mL of DMSO, respectively, and held at 100 °C (or 150 °C) for 6 h, and GS-MS was applied to monitor this reaction (**Fig. 10b**). The peak at around 17.7 min corresponds to DBH, and the peak at around 19.3 min represents BMH. After reaction at 100 °C for 6 h, there was no additional peak produced. Thus, the hydrazone metathesis of DBH and BMH could not occur at 100 °C, which suggests that the hydrazone group is a thermally stable group at temperature ≤ 100 °C, corresponding to the high initial creep temperature. When the temperature rose to 150 °C, there appeared a strong peak at around 18.4 min representing a new dihydrazone BMBH. In other words, the hydrazone metathesis of DBH and BMH could proceed smoothly at 150 °C, which makes it possible for HBE-D400 and HBE-IPDA to relax and achieve network rearrangement at relatively high temperatures.

View Article Online
DOI: 10.1039/C9TA119B

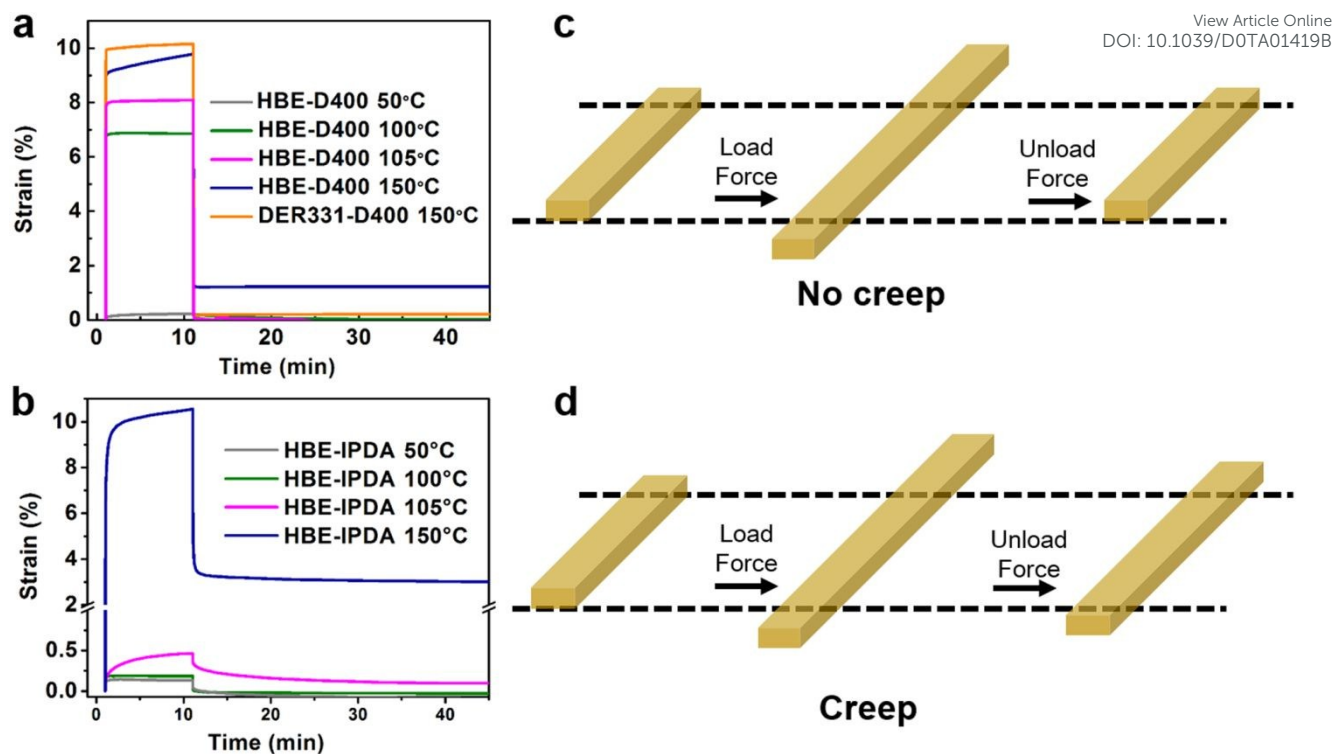


Fig. 9 Creep tests of a) HBE-D400 and DER331-D400, b) HBE-IPDA at different temperatures under 1 MPa stress. c-d) Diagrams of the samples with c) no creep and d) creep during the creep tests.

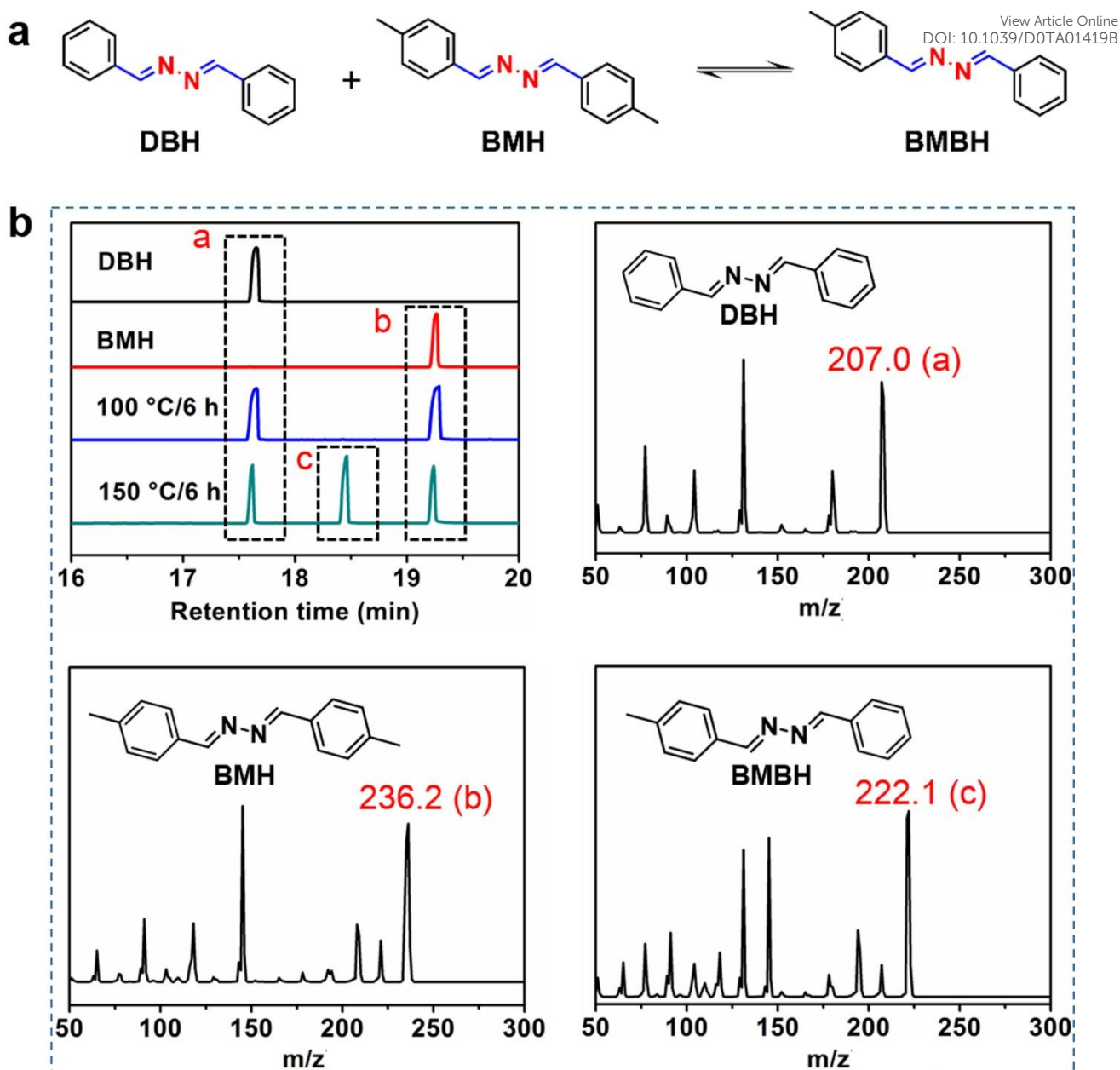


Fig. 10 Dihydrazone exchange reaction. a) Model reaction between small-molecule model dihydrazones DBH and BMH. b) GC-MS spectra of the equilibration of DBH and BMH to BMBH at 100 °C and 150 °C, respectively.

3.4 Reprocessing Recyclability of the dihydrazone CANs

Reprocessing recyclability is a paramount feature of CANs. Despite the great creep resistance of HBE-D400 and HBE-IPDA, these materials could still be reprocessed in tens of minutes at 180 °C (Fig. 11a and Fig. S4). Take HBE-D400 as an example, pieces of sample could be recovered into complete films via hot pressing within 45 min at 180 °C under a pressure of 10 MPa. After reprocessing, the chemical structures of the CANs preserved

well, which could be seen from the FT IR spectra of the original and reprocessed CANs in Fig. 11b. As seen in Fig. 11c, there was only slightly decrease of the mechanical properties, which might be attributed to the unrecoverable chain scission within the network during the repeated chopping and hot-pressing molding,³⁶ and after further reprocessing for three times, the mechanical properties of the CANs still maintained well. Take HBE-IPDA as an example, the sample reprocessed for three times maintained 92.6% tensile strength of the original one (Fig. S5, Table S1). For conventional Schiff base CANs, the modulus would be increased on account of the oxidation¹⁶ or self-cross-linking of Schiff base,⁶⁶ while for the dihydrazone CANs, the modulus was not increased, which suggests that dihydrazone is relatively stable at high temperature.

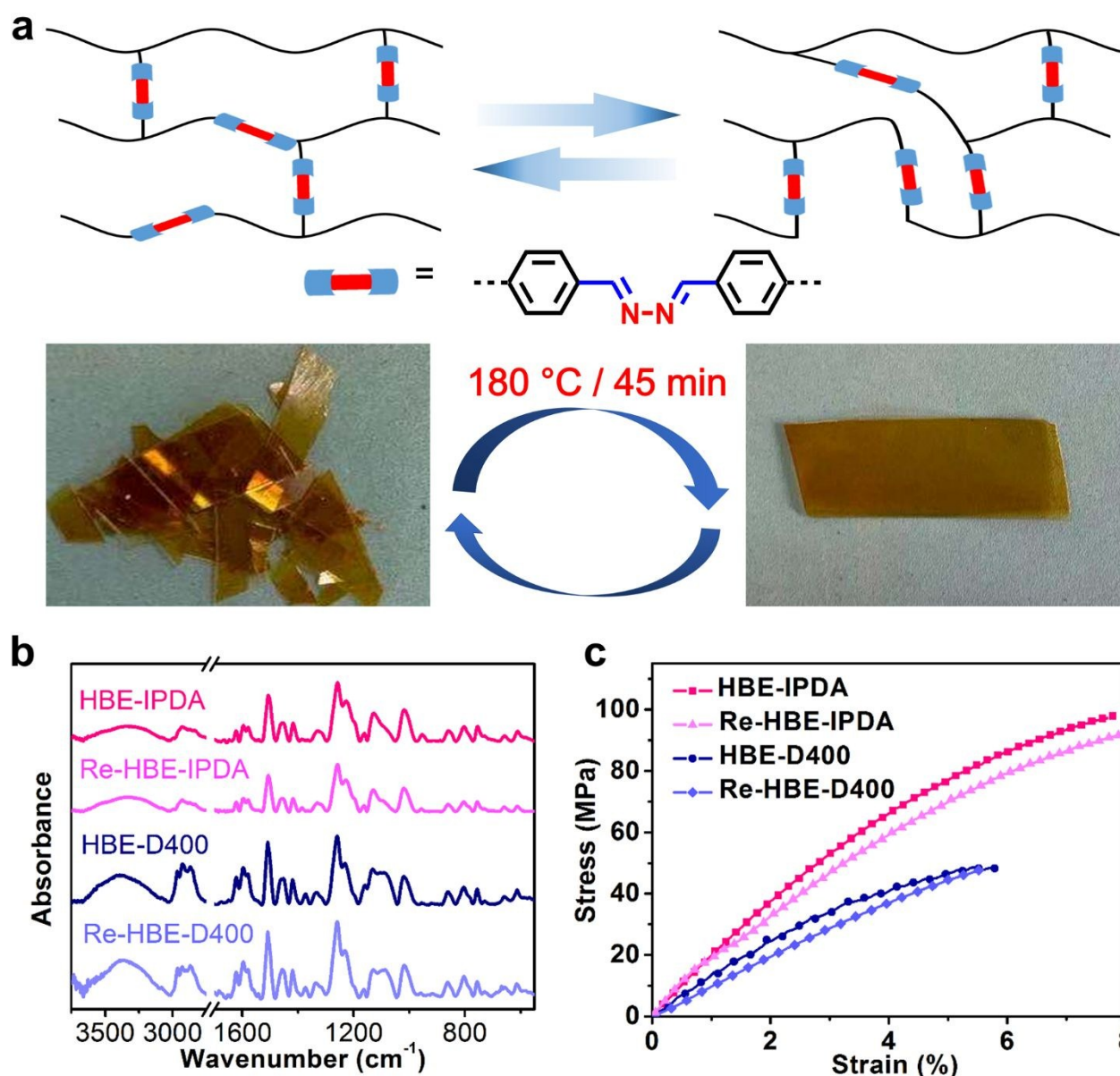


Fig. 11 a) Reprocess of HBE-D400 at 180 °C for 45 min under a pressure of 10 MPa. b) FT IR spectra of the original and reprocessed HBE-IPDA and HBE-D400. c) Representative tensile stress-strain curves of the

original and reprocessed HBE-IPDA and HBE-D400.

View Article Online
DOI: 10.1039/D0TA01419B

3.5 Degradation of the dihydrazone CANs

The degradation performances of HBE-D400 and HBE-IPDA were characterized by adjusting temperature, acid type, acid concentration and solvent. As shown in **Fig. 12a** and **Fig. S6**, the degradation of HBE-D400 and HBE-IPDA presented obvious temperature dependence. Degradation could proceed smoothly at 50 °C with a fast rate. For example, HBE-D400 could be degraded and completely dissolved in 0.1 M HCl acetone/water (8/2, v/v) solution within 2 h at 50 °C, while almost no degradation occurred at 23 °C for 48 h. Same phenomenon occurred for HBE-IPDA. In addition to temperature dependence, the degradation of HBE-D400 and HBE-IPDA also exhibited certain selectivity to organic solvents. Acetone, methanol, DMSO and so on could significantly accelerate the degradation process (**Fig. 12b** and **Fig. S7**). With the high acceleration efficiency and relatively green feature, acetone was selected as the main solvent in the degradation experiments. It can be observed from **Fig. 12c** and **Fig. S8** that the degradations of HBE-D400 and HBE-IPDA exhibited acidity dependence. The degradations of the dihydrazone CANs were fast in 0.2 M and 0.1 M HCl solutions and 0.1 M H₂SO₄ solution, when decreasing the acid concentration to 0.05 M and 0.01 M or replacing HCl (or H₂SO₄) with weaker acids, the degradation rate was greatly reduced. This manifests that the acid could catalyze the degradation of hydrazone bond. Besides, the ratio of water to main solvent in acid solution exhibited great influence on the degradation. Take 0.1 M HCl water/acetone solution as an example (**Fig. 12d** and **Fig. S9**), when the ratio of water to acetone was 1:9 or 2:8, the degradation rate was fast. As the water content increased, the rate of degradation decreased, and when the water content was greater than 60%, the degradation hardly proceeded. With increasing the water content, the solubility of degraded products and the wettability toward the samples reduced, thus, exhibited a negatively effect on the degradation.^{48, 67}

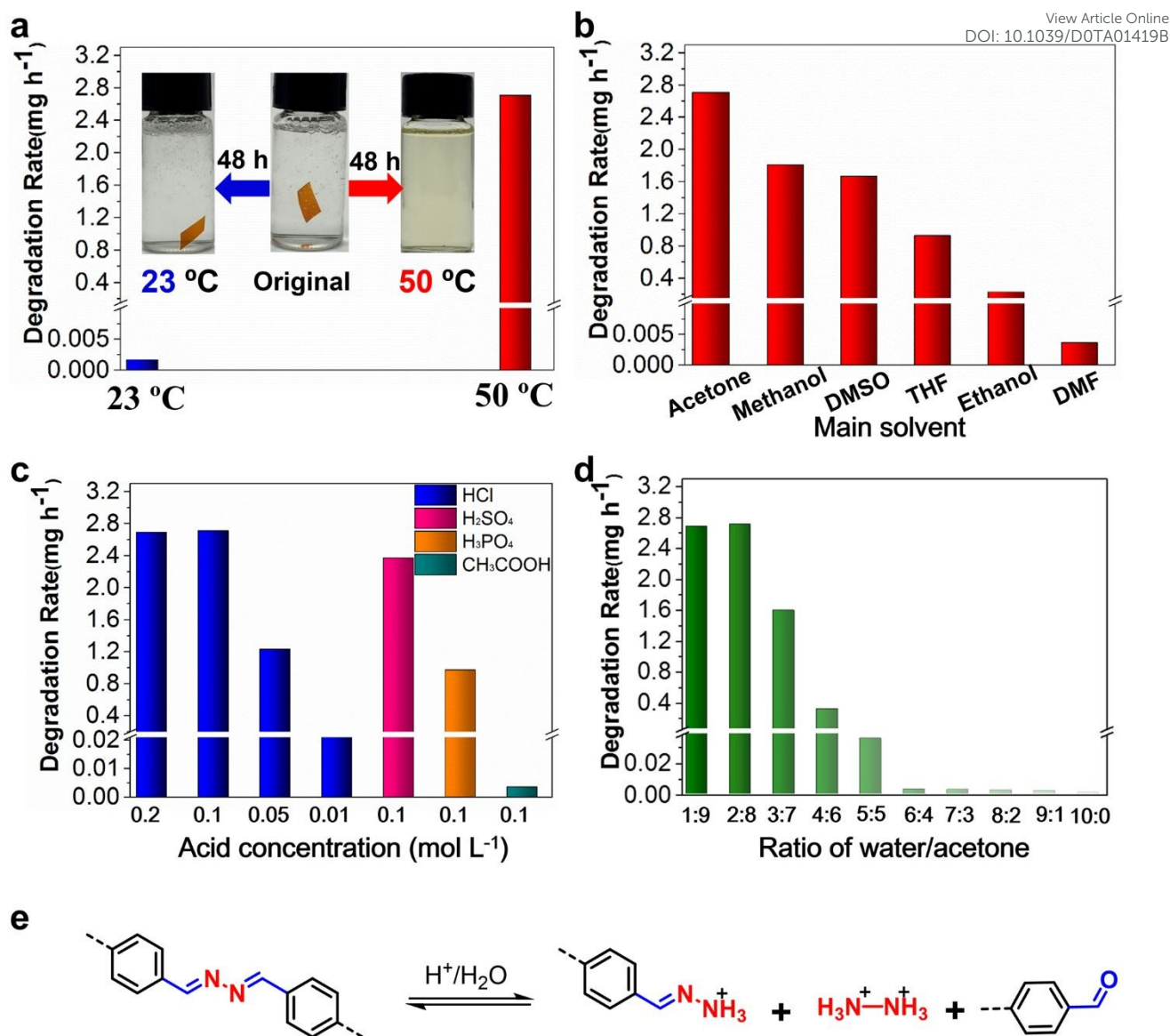


Fig. 12 Degradation of HBE-D400. a) Different degradation rate in 0.1 M HCl water/acetone (2/8, v/v) solution at 23 °C and 50 °C. b) Degradation rate in 0.1 M HCl water/main solvent (2/8, v/v) solution with different main solvent at 50 °C. c-d) Degradation rate in c) different acid water/acetone (2/8, v/v) solutions and d) 0.1 M HCl water/acetone solutions with different solvent ratios at 50 °C. e) Degradation mechanism of the dihydrazone CANs.

In order to explore the degradation mechanism of the dihydrazone CANs. The small-molecule model dihydrazone DBH (~2 mg) was used to detect the degradation of dihydrazone structure under acidic condition (1 mL, 0.1 M HCl water/DMSO-d₆ (2/8, v/v) solution) at 23 °C. Since hydrazine hydrate is a binary weak base, the corresponding dihydrazone structure in DBH was degraded in two steps (Fig. S10) of i) acid-catalyzed hydrolysis into monohydrazone, ii) further hydrolysis of monohydrazone. Even so, DBH could be completely degraded quickly in the presence of a sufficient amount of acid. In other words, hydrazone group possesses

excellent degradability in acidic environment. During the degradation, dihydrazone CANs were first degraded into oligomers and dissolved in the degradation solution. As the degradation time increased, the dihydrazone groups in the oligomers would further degrade. The degradation process of dihydrazone CANs (take HBE-IPDA as an example) was also monitored by ^1H NMR spectra (Fig. S11), there appeared peaks for aldehyde and monohydrazone, and the peak strength for aldehyde is much stronger than that for monohydrazone. This suggests that the dihydrazone CANs demonstrated similar degradation process to DBH (Fig. S11), and the degradation mechanism of the dihydrazone CANs can be summarized as Fig. 12e.

Static contact angle and swelling tests were performed to explain the degradation phenomena described above. As shown in Table 3, Table S2, Fig. S12 and Fig. S13, the contact angle decreased with the increase of the acetone content, and the contact angle also changed as the main solvent, which manifests that the wettability of the acid solutions on these materials varied with the different solvents, corresponding to the different degradation rates. The better wettability tended to bring about faster degradation. The swelling tests also presented the same results. In addition, the swelling degree of HEB-D400 increased significantly in the same solvent (water/acetone (v/v) = 2 : 8) as the degradation temperature increased from 23 °C to 50 °C (Table 3 and Table S2). The solvent was arduous to penetrate the networks at 23 °C, however, this process would occur smoothly at 50 °C, as a result, these networks kept stable at 23 °C and could be degraded quickly at 50 °C.

Table 3 Contact angle and swelling degree of HEB-D400 in different solvents at 50 °C.

Main solvent	Methanol	Ethanol	THF	DMSO	DMF	Acetone									
						10/0	9/1	8/2	7/3	6/4	5/5	4/6	3/7	2/8	1/9
Water/Main solvent, (v/v)	2/8	2/8	2/8	2/8	2/8	10/0	9/1	8/2	7/3	6/4	5/5	4/6	3/7	2/8	1/9
Contact angle (°)	31.4	35.9	20.5	23.9	44.0	78.1	77.3	66.9	62.3	50.9	38.9	40.1	33.4	27.7	21.1
Swelling degree (%)	31	14	21	28	2	1	2	6	11	17	23	27	30	34 (2*)	38

*: Swelling test at 23 °C

3.6 Antibacterial properties of the dihydrazone CANs

Hydrazone group has a good antibacterial effect,^{68, 69} however, little research has been done for thermosets containing hydrazone group. In this work, Gram-negative bacteria (*E. coli*) (a kind of bacteria which is very

common in our life) was used to test the bactericidal effect of HBE-D400 and DER331-D400. As seen from **Fig. 13**, DER331-D400 exhibited almost no antibacterial effect, and there were lots of green dots representing the lived bacteria and almost no red dots representing the dead bacteria. However, HBE-D400 exhibited an opposite phenomenon, a large number of red dots and almost no green dots were on the typical fluorescent image. Therefore, the dihydrazone CANs possessed excellent antibacterial properties. Beside the contribution from the hydrazine group, the methoxy group on HBE should also have some contribution to the excellent bactericidal efficiency.⁴⁸ The killing rate of HBE-D400 toward *E. coli* was as high as 95.8%, which makes it as potential intrinsically antibacterial materials.

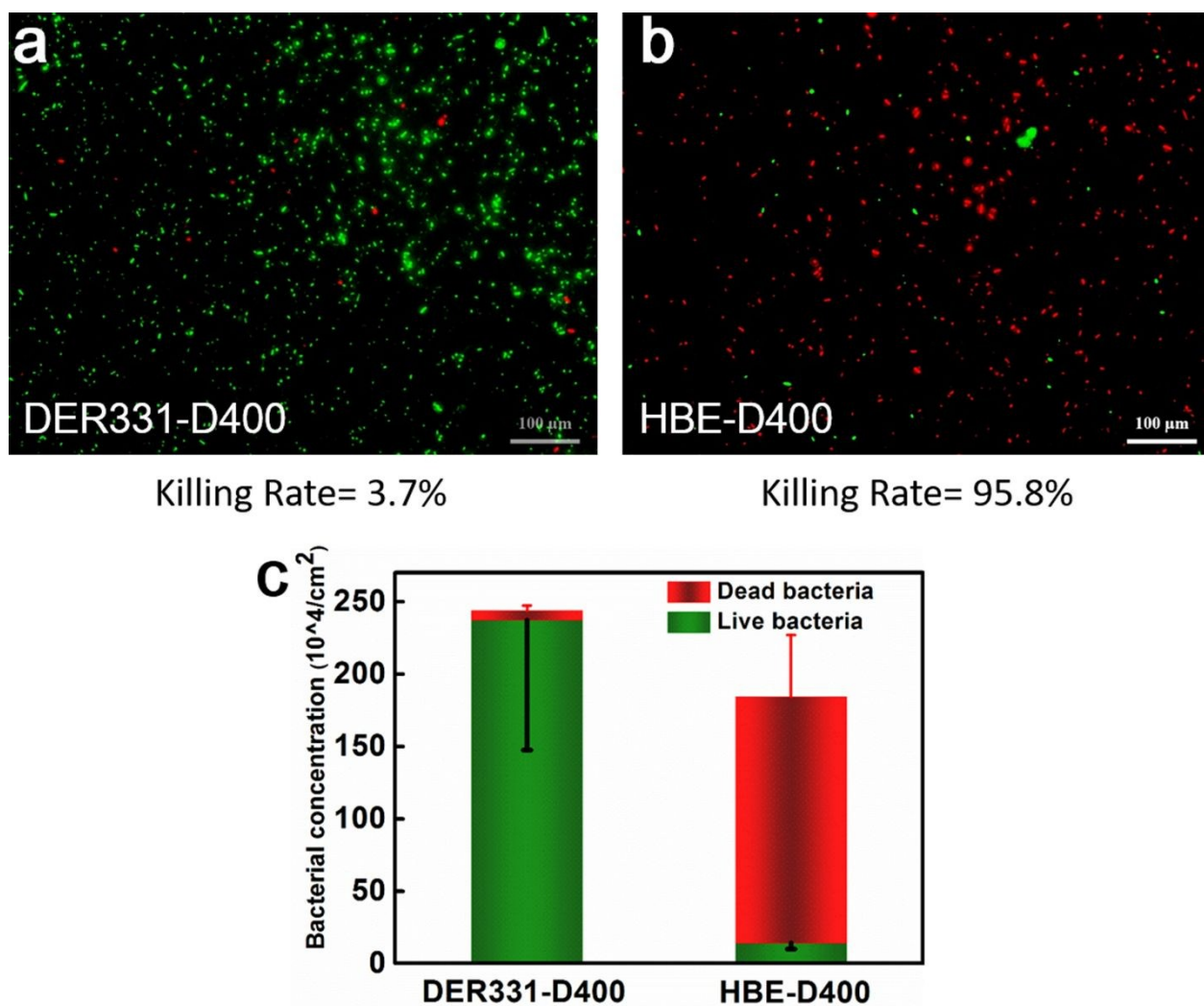


Fig. 13 Fluorescence microscopy images of *E. coli* on coatings based on a) DER331-D400, b) HBE-D400; c) Bacteria concentration and killing rate of DER331-D400 and HBE-D400 toward *E. coli*.

4. Conclusions

A novel dihydrazone-containing epoxy monomer was successfully synthesized from vanillin and hydrazinium

hydrate, followed by reacting with epichlorohydrin. The epoxy was further cross-linked with a soft-hardener and a rigid hardener to achieve two dihydrazone CANs, respectively. On account of the stable feature at temperature of around 100 °C and excellent exchangeability of hydrazone bond, the dihydrazone CANs could not proceed creep even at high temperature of ~105 °C and presented superior malleability and reprocessability. In addition, both CANs exhibited evident command degradability reflected from their temperature, solvent and acidity dependence, and the dihydrazone structure in networks followed two-step degradation mechanism of i) acid-catalyzed hydrolysis into monohydrazone, ii) further hydrolysis of monohydrazone. Moreover, owing to the high antibacterial feature of hydrazone bond and methoxy group on vanillin, the CANs presented high killing rate (95.8%) to Gram-negative bacteria (*E. coli*). This work provides a promising dynamic covalent motif to develop CANs which had great potential to be as recyclable and intrinsic antibacterial engineering plastics or structure materials.

Conflicts of interest

There are no conflicts to declare.

Acknowledgements

The authors thank the financial support from National Natural Science Foundation of China (No. 51773216), Youth Innovation Promotion Association, CAS (No. 2018335), and Natural Science Foundation of Zhejiang Province (No. LQ20E030005).

Notes and References

- 1 J.-S. Chen, C. K. Ober and M. D. Poliks, *Polymer*, 2002, **43**, 131-139.
- 2 S. Yang, J.-S. Chen, H. Körner, T. Breiner, C. K. Ober and M. D. Poliks, *Chemistry of Materials*, 1998, **10**, 1475-1482.
- 3 S. Ma and D. C. Webster, *Prog. Polym. Sci.*, 2018, **76**, 65-110.
- 4 P. R. Christensen, A. M. Scheuermann, K. E. Loeffler and B. A. Helms, *Nature Chemistry*, 2019, **11**, 442-448.
- 5 D. Montarnal, M. Capelot, F. Tournilhac and L. Leibler, *Science*, 2011, **334**, 965-968.
- 6 H. Sardon and A. P. Dove, *Science*, 2018, **360**, 380-381.
- 7 J. M. García, G. O. Jones, K. Virwani, B. D. McCloskey, D. J. Boday, G. M. ter Huurne, H. W. Horn, D. J. Coady, A. M. Bintaleb, A. M. S. Alabdulrahman, F. Alsewaleim, H. A. A. Almegren and J. L. Hedrick, *Science*, 2014, **344**, 732.
- 8 W. Post, A. Susa, R. Blaauw, K. Molenveld and R. J. I. Knoop, *Polym. Rev.*, 2020, **60**, 359-388.
- 9 M. Capelot, D. Montarnal, F. Tournilhac and L. Leibler, *J. Am. Chem. Soc.*, 2012, **134**, 7664-7667.

- 10 Z. Pei, Y. Yang, Q. Chen, E. M. Terentjev, Y. Wei and Y. Ji, *Nat. Mater.*, 2014, **13**, 36-41.
- 11 J. P. Brutman, P. A. Delgado and M. A. Hillmyer, *ACS Macro Lett.*, 2014, **3**, 607-610.
- 12 E. Trovatti, T. M. Lacerda, A. J. F. Carvalho and A. Gandini, *Adv. Mater.*, 2015, **27**, 2242-2245.
- 13 X. X. Chen, M. A. Dam, K. Ono, A. Mal, H. B. Shen, S. R. Nutt, K. Sheran and F. Wudl, *Science*, 2002, **295**, 1698-1702.
- 14 P. Taynton, K. Yu, R. K. Shoemaker, Y. Jin, H. J. Qi and W. Zhang, *Adv. Mater.*, 2014, **26**, 3938-3942.
- 15 P. Taynton, H. Ni, C. Zhu, K. Yu, S. Loob, Y. Jin, H. J. Qi and W. Zhang, *Adv. Mater.*, 2016, **28**, 2904-2909.
- 16 S. Wang, S. Ma, Q. Li, X. Xu, B. Wang, W. Yuan, S. Zhou, S. You and J. Zhu, *Green Chem.*, 2019, **21**, 1484-1497.
- 17 O. R. Cromwell, J. Chung and Z. Guan, *J. Am. Chem. Soc.*, 2015, **137**, 6492-6495.
- 18 W. A. Ogden and Z. Guan, *J. Am. Chem. Soc.*, 2018, **140**, 6217-6220.
- 19 M. Röttger, T. Domenech, R. van der Weegen, A. Breuillac, R. Nicolaÿ and L. Leibler, *Science*, 2017, **356**, 62-65.
- 20 M. Guerre, C. Taplan, R. Nicolaÿ, J. M. Winne and F. E. Du Prez, *J. Am. Chem. Soc.*, 2018, **140**, 13272-13284.
- 21 W. Denissen, I. De Baere, W. Van Paepegem, L. Leibler, J. Winne and F. E. Du Prez, *Macromolecules*, 2018, **51**, 2054-2064.
- 22 W. Denissen, G. Rivero, R. Nicolaÿ, L. Leibler, J. M. Winne and F. E. Du Prez, *Adv. Funct. Mater.*, 2015, **25**, 2451-2457.
- 23 W. Denissen, M. Droesbeke, R. Nicolaÿ, L. Leibler, J. M. Winne and F. E. Du Prez, *Nat. Commun.*, 2017, **8**, 14857.
- 24 Y.-X. Lu, F. Tournilhac, L. Leibler and Z. Guan, *J. Am. Chem. Soc.*, 2012, **134**, 8424-8427.
- 25 W.-X. Liu, C. Zhang, H. Zhang, N. Zhao, Z.-X. Yu and J. Xu, *J. Am. Chem. Soc.*, 2017, **139**, 8678-8684.
- 26 C. Taplan, M. Guerre, J. M. Winne and F. E. Du Prez, *Mater. Horiz.*, 2020, **7**, 104-110.
- 27 R. L. Snyder, D. J. Fortman, G. X. De Hoe, M. A. Hillmyer and W. R. Dichtel, *Macromolecules*, 2018, **51**, 389-397.
- 28 H. Lei, S. Wang, D. J. Liaw, Y. Cheng, X. Yang, J. Tan, X. Chen, J. Gu and Y. Zhang, *ACS Macro Lett.*, 2019, 582-587.
- 29 J. Tang, L. Wan, Y. Zhou, H. Pan and F. Huang, *J. Mater. Chem. A*, 2017, **5**, 21169-21177.
- 30 M. M. Obadia, B. P. Mudraboyina, A. Sergeï, D. Montarnal and E. Drockenmuller, *J. Am. Chem. Soc.*, 2015, **137**, 6078-6083.
- 31 B. Hendriks, J. Waelkens, J. M. Winne and F. E. Du Prez, *ACS Macro Lett.*, 2017, **6**, 930-934.
- 32 S.-M. Kim, H. Jeon, S.-H. Shin, S.-A. Park, J. Jegal, S. Y. Hwang, D. X. Oh and J. Park, *Adv. Mater.*, 2018, **30**, 1705145.
- 33 X. Wu, X. Yang, W. Huang, R. Yu, X. Zhao and Y. Zhang, *J. Mater. Chem. A*, 2018, **22**, 10184-10188.
- 34 C. A. Tretbar, J. A. Neal and Z. Guan, *J. Am. Chem. Soc.*, 2019, **141**, 16595-16599.
- 35 Y. Nishimura, J. Chung, H. Muradyan and Z. Guan, *J. Am. Chem. Soc.*, 2017, **139**, 14881-14884.
- 36 S. Wu, Z. Yang, S. Fang, Z. Tang, F. Liu and B. Guo, *J. Mater. Chem. A*, 2019, **7**, 1459-1467.
- 37 S. Ji, F. Fan, C. Sun, Y. Yu and H. Xu, *ACS Appl. Mater. Inter.*, 2017, **9**, 33169-33175.
- 38 N. Van Herck, D. Maes, K. Unal, M. Guerre, J. M. Winne and F. E. Du Prez, *Angew. Chem. Int. Ed.*, 2020, **59**, 3609-3617.
- 39 H. Ying, Y. Zhang and J. Cheng, *Nat. Commun.*, 2014, **5**, 3218.
- 40 Q. Li, S. Ma, S. Wang, W. Yuan, X. Xu, B. Wang, K. Huang and J. Zhu, *J. Mater. Chem. A*, 2019, **7**, 18039-18049.
- 41 Q. Li, S. Ma, S. Wang, Y. Liu, M. A. Taher, B. Wang, K. Huang, X. Xu, Y. Han and J. Zhu, *Macromolecules*, 2020, **53**, 1474-1485.
- 42 Q. Zhang, X. Zhu, C.-H. Li, Y. Cai, X. Jia and Z. Bao, *Macromolecules*, 2019, **52**, 660-668.
- 43 J. J. Cash, T. Kubo, D. J. Dobbins and B. S. Sumerlin, *Polym. Chem.*, 2018, **9**, 2011-2020.
- 44 L. Li, X. Chen, K. Jin and J. M. Torkelson, *Macromolecules*, 2018, **51**, 5537-5546.
- 45 Y. Liu, Z. Tang, D. Wang, S. Wu and B. Guo, *J. Mater. Chem. A*, 2019, **7**, 26867-26876.
- 46 M. Capelot, M. M. Unterlass, F. Tournilhac and L. Leibler, *ACS Macro Lett.*, 2012, **1**, 789-792.
- 47 J. J. Lessard, G. M. Scheutz, S. H. Sung, K. A. Lantz, T. H. Epps and B. S. Sumerlin, *J. Am. Chem. Soc.*, 2020, **142**, 283-289.
- 48 X. Xu, S. Ma, J. Wu, J. Yang, B. Wang, S. Wang, Q. Li, J. Feng, S. You and J. Zhu, *J. Mater. Chem. A*, 2019, **7**, 15420-15431.
- 49 K. Bush, P. Courvalin, G. Dantas, J. Davies, B. Eisenstein, P. Huovinen, G. A. Jacoby, R. Kishony, B. N. Kreiswirth and E. Kutter, *Nat. Rev. Microbiol.*, 2011, **9**, 894-896.

- 50 E. G. Pamer, *Science*, 2016, **352**, 535-538.
- 51 R. López-Igual, J. Bernal-Bayard, A. Rodríguez-Patón, J.-M. Ghigo and D. Mazel, *Nat. Biotechnol.*, 2019, **37**, 755-760.
- 52 Y. Ding, Z. Sun, R. Shi, H. Cui, Y. Liu, H. Mao, B. Wang, D. Zhu and F. Yan, *ACS Appl. Mater. Inter.*, 2018, **11**, 2860-2869.
- 53 D. Pranantyo, L. Q. Xu, E.-T. Kang and M. B. Chan-Park, *Biomacromolecules*, 2018, **19**, 2156-2165.
- 54 A. Żywicka, K. Fijałkowski, A. F. Junka, J. Grzesiak and M. El Fray, *Biomacromolecules*, 2018, **19**, 1528-1538.
- 55 H. Xu, Z. Fang, W. Tian, Y. Wang, Q. Ye, L. Zhang and J. Cai, *Adv. Mater.*, 2018, **30**, 1801100.
- 56 D. Gan, T. Xu, W. Xing, X. Ge, L. Fang, K. Wang, F. Ren and X. Lu, *Adv. Funct. Mater.*, 2019, **29**, 1805964.
- 57 P. Yan, W. Zhao, Y. Wang, Y. Jiang, C. Zhou and J. Lei, *Macromol. Chem. Phys.*, 2017, **218**, 1700265-n/a.
- 58 V. Lázár, A. Martins, R. Spohn, L. Daruka, G. Grézal, G. Fekete, M. Számel, P. K. Jangir, B. Kintses and B. Csörgő, *Nat. Microbiol.*, 2018, **3**, 718-731.
- 59 N. Hao, K. W. Jayawardana, X. Chen and M. Yan, *ACS Appl. Mater. Inter.*, 2015, **7**, 1040-1045.
- 60 B. Peng, X. Zhang, D. G. A. L. Aarts and R. P. A. Dullens, *Nat. Nanotechnol.*, 2018, **13**, 478-482.
- 61 B. Lee, K. H. Lee, J. Cho, W. Nam and N. H. Hur, *Org. Lett.*, 2011, **13**, 6386-6389.
- 62 T. Hashimoto, H. Meiji, M. Urushisaki, T. Sakaguchi, K. Kawabe, C. Tsuchida and K. Kondo, *J. Polym. Sci., Part A: Polym. Chem.*, 2012, **50**, 3674-3681.
- 63 K. E. Boehle, J. Gilliland, C. R. Wheeldon, A. Holder, J. A. Adkins, B. J. Geiss, E. P. Ryan and C. S. Henry, *Angew. Chem. Int. Ed.*, 2017, **56**, 6886-6890.
- 64 S. Ma and D. C. Webster, *Macromolecules*, 2015, **48**, 7127-7137.
- 65 S.-A. Park, H. Jeon, H. Kim, S.-H. Shin, S. Choy, D. S. Hwang, J. M. Koo, J. Jegal, S. Y. Hwang, J. Park and D. X. Oh, *Nat. Commun.*, 2019, **10**, 2601.
- 66 J.-N. Wu, L. Chen, T. Fu, H.-B. Zhao, D.-M. Guo, X.-L. Wang and Y.-Z. Wang, *Chem. Eng. J.*, 2018, **336**, 622-632.
- 67 B. Wang, S. Ma, Q. Li, H. Zhang, J. Liu, R. Wang, Z. Chen, X. Xu, S. Wang, N. Lu, Y. Liu, S. Yan and J. Zhu, *Green Chem.*, 2020, **22**, 1275-1290.
- 68 Y. Imashiro, K. Masuda In *Japan Patent 6932411*, 1969, 1970; p 111482q
- 69 M.-H. Shih and F.-Y. Ke, *Biorg. Med. Chem.*, 2004, **12**, 4633-4643.

View Article Online
DOI: 10.1039/D0TA01419B

Table of Contents Entry

Dihydrazone-based Dynamic Covalent Epoxy Networks with High Creep Resistance, Controlled Degradability, and Intrinsic Antibacteria from Bioresources

Xiwei Xu, Songqi Ma,* Sheng Wang, Jiahui Wu, Qiong Li, Na Lu, Yanlin liu, Jintao Yang, Jie Feng, Jin Zhu



This work highlights the exploitation of dihydrazone motif to build antibacterial covalent adaptable networks with no creep at ~ 105 °C.